Chemical Science

ROYAL SOCIETY OF CHEMISTRY

EDGE ARTICLE

View Article Online
View Journal | View Issue

Cite this: *Chem. Sci.*, 2021, **12**, 11045

All publication charges for this article have been paid for by the Royal Society of Chemistry

Received 6th May 2021
Accepted 15th July 2021

DOI: 10.1039/d1sc02497c

rsc.li/chemical-science

A mesoporous ionic solid with 272 $Au^{I}_{6}Ag^{I}_{3}Cu^{II}_{3}$ complex cations in a super huge crystal lattice†

Hiroto Takeda, Tatsuhiro Kojima, Nobuto Yoshinari and Takumi Konno *

Here, we report a unique mesoporous ionic solid (I) generated from a cationic $Au^{I}_{6}Ag^{I}_{3}Cu^{II}_{3}$ dodecanuclear complex with D-penicillamine depending on the homochirality and crystallization conditions. I crystallizes in the cubic space group of $F4_132$ with an extremely large cell volume of 2 171 340 $Å^3$, containing 272 $Au^{I}_{6}Ag^{I}_{3}Cu^{II}_{3}$ complex cations in the unit cell. In I, the complex cations are connected to each other through CH···π interactions in a zeotype framework, the topology of which is the same as that of the metal–organic framework in MIL-101, with similar but much larger two types of polyhedral pores with internal diameters of 38.2 Å and 49.7 Å, which are occupied by counter-anions and water molecules. Due to the cationic nature of the framework, I undergoes quick, specific exchanges of counter-anions while retaining its single crystallinity. This study realized the creation of a non-covalent mesoporous framework from a single complex salt, providing a conceptual advance in solid chemistry and material science.

Introduction

Recent increased interest in porous crystalline materials in chemistry and material science stems from the versatile applications of these materials in, for example, heterogeneous catalysis,[1,2] storage and separation of molecules[3–6] and ion exchange of ionic species.[7–10] The availability of framework pores in crystalline materials as reaction fields to generate chemical species that cannot be obtained *via* conventional approaches,[2,7–10] together with the incorporation and structural determination of molecules that are hardly crystallized,[11–13] has also inspired the recent considerable attention to this class of materials. While high porosities and low material densities are needed for the efficient storage and separation of small molecules such as gases and vapors,[3,6] other applications also require open channels and pore volumes that are suitable for the sizes of guest molecules, allowing fast diffusion, transfer and specific adsorption in the pores.[4,6,14] Thus, the creation of artificial crystalline materials with mesopores with diameters of 2 nm to 50 nm is highly desirable for use in a wide range of applications, such as controlled synthesis of nanoparticles,[15] immobilization of biomolecules for catalysts[16] and capillary condensation of gaseous molecules,[16–18] which are not possible for microporous materials with diameters less than 2 nm and macroporous materials with diameters greater than 50 nm.

In 2002, Eddaoudi *et al.* reported the first crystalline material with three-dimensional (3D) mesopores with a diameter of 2.9 nm, named IRMOF-16, which is a metal–organic framework (MOF) sustained by coordination bonds between Zn^{II}_{4} nodes and dicarboxylate linkers.[19] Since then, a number of mesoporous crystalline materials with MOF structures have been synthesized based on the hierarchical self-assembly of molecular nodes and linkers using a synthetic strategy similar to that applied for IRMOF-16.[20–25] One of the well-known examples of this class of materials is MIL-101, whose zeotype framework is composed of Cr^{III}_{3} nodes and dicarboxylate linkers to form two kinds of cage-type mesopores with diameters of 2.9 nm and 3.4 nm.[26] More recently, a unique crystalline MOF with larger mesopores with diameters of 5.0 nm and 6.2 nm, named NU-1301, has also been synthesized *via* the combination of UO_2^{2+} nodes and tricarboxylate linkers.[27] Thus, rigid, directional coordination bonds between metal centres and carboxylate ligands have been critical for the creation of mesoporous crystalline compounds, although mesoporous frameworks sustained by covalent bonds and hydrogen bonds have been observed in organic solid materials.[28–35]

Here, we report the first mesoporous framework sustained by non-covalent CH···π interactions in a non-MOF coordination system, the structure of which was established by single-crystal X-ray crystallography. This system consists of a newly prepared $Au^{I}_{6}Ag^{I}_{3}Cu^{II}_{3}$ dodecanuclear complex salt, $[Au_6Ag_3Cu_3(tdme)_2(D\text{-}pen)_6](TFA)_3$ (tdme = 1,1,1-tris(diphenylphosphinomethyl)

Department of Chemistry, Graduate School of Science, Osaka University, Toyonaka, Osaka, Japan. E-mail: konno@chem.sci.osaka-u.ac.jp

† Electronic supplementary information (ESI) available: Experimental detail, PXRD, and XRF, IR, adsorption, diffuse reflectance, and CD spectra, as well as crystal structures and crystallographic data. CCDC 2024986–2024990. For ESI and crystallographic data in CIF or other electronic format see DOI: 10.1039/d1sc02497c

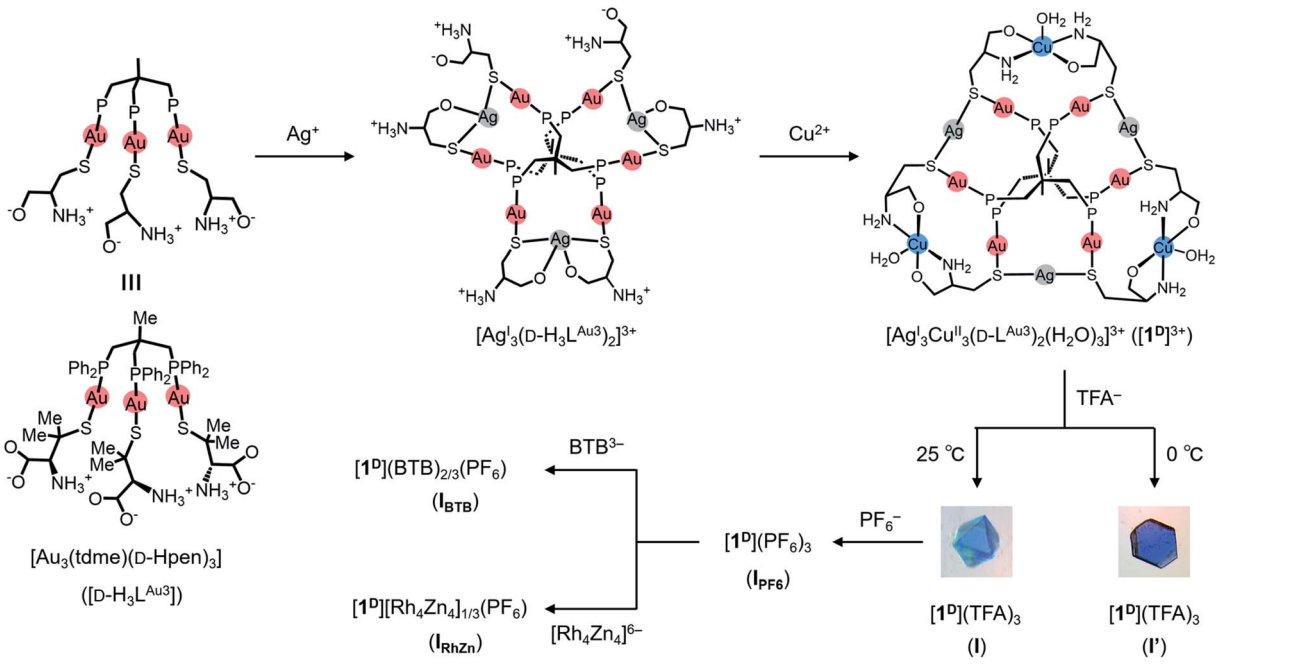

Fig. 1 Synthetic routes of I′, I, I_{PF6}, I_{BTB}, and I_{RhZn}.

ethane, D-H_2pen = D-penicillamine, TFA = trifluoroacetate), which crystallizes in a 3D ionic solid (**I**) with a very large unit cell containing a total of 272 $Au^I_6Ag^I_3Cu^{II}_3$ complex cations. Notably, the framework of **I** has the same topology as that of MIL-101, forming two kinds of cage-type mesopores that are larger than those in MIL-101, although the framework is composed of only complex cations linked by intermolecular CH$\cdots\pi$ interactions rather than coordination bonds, with its voids being occupied by counter-anions and water molecules. **I** is a kinetic product crystallized from aqueous media under ambient conditions and is reproducible and interconvertible with the thermodynamic non-porous solid product (**I′**) just by changing the crystallization temperature (Fig. 1). Very fast and specific anion exchanges for **I**, along with the creation of an analogous ionic solid (**II**) with smaller mesopores by introducing DL-pen instead of D-pen, are also reported.

Results and discussion, experimental

Synthesis, characterization and crystal structure of I′

As a continuation of our recent work on the creation of multinuclear coordination compounds based on the trigold(I) metalloligand with a mixture of hydrophobic 1,1,1-tris(diphenylphosphinomethyl)ethane (tdme) and hydrophilic D-penicillamine (D-H_2pen), [Au_3(tdme)(D-Hpen)$_3$] (D-$H_3L^{Au_3}$),[36–38] D-$H_3L^{Au_3}$ was treated with 1.5 equiv. of silver(I) trifluoroacetate in MeOH/CH_3CN at 0 °C. This treatment yielded a colourless solution, from which colourless stick crystals were isolated upon addition of aqueous sodium nitrate. Single-crystal X-ray crystallography (Fig. S1 and Table S1†), together with the X-ray fluorescence (Fig. S2†) and elemental analyses, indicated that the colourless crystals contain the $Au^I_6Ag^I_3$ nonanuclear complex with free ammonium groups, $[Ag_3(D\text{-}H_3L^{Au_3})_2]^{3+}$, in which two D-$H_3L^{Au_3}$ metalloligands are spanned by three Ag^I ions through thiolato and carboxylate groups (Fig. S1†).

Further treatment of the colourless solution obtained from D-$H_3L^{Au_3}$ and silver(I) trifluoroacetate with 1.5 equiv. of aqueous copper(II) acetate at 0 °C yielded a blue solution, from which X-ray-quality blue crystals with a hexagonal plate shape (**I′**) were obtained by slow evaporation at 0 °C. Based on the IR spectrum (Fig. S3†) and the X-ray fluorescence and elemental analyses, **I′** was assigned as an $Au^I_6Ag^I_3Cu^{II}_3$ dodecanuclear complex with the chemical formula $[Ag_3Cu_3(D\text{-}L^{Au_3})_2](TFA)_3\cdot nH_2O$. The diffuse reflection spectrum of **I′** exhibits a broad d–d band at 630 nm due to Cu^{II} centers[39] and a positive band is observed in the solid-state CD spectrum in this region (Fig. S4†), indicative of the optically active nature of **I′**.

The structure of **I′** was established by single-crystal X-ray crystallography, which revealed the presence of complex cations ($[\mathbf{1^D}]^{3+} = [Ag_3Cu_3(D\text{-}L^{Au_3})_2(H_2O)_3]^{3+}$) and TFA^- anions in a 1 : 3 ratio. As shown in Fig. 2a and b, the complex cation $[\mathbf{1^D}]^{3+}$ contains two $(D\text{-}L^{Au_3})^{3-}$ metalloligands that are spanned by 3 Ag^I atoms through thiolato groups and by 3 Cu^{II} atoms through amine and carboxylate groups, forming the cage-type $Au^I_6Ag^I_3Cu^{II}_3$ dodecanuclear structure in $[Ag^I_3Cu^{II}_3(D\text{-}L^{Au_3})_2(H_2O)_3]^{3+}$. The overall structure in $[\mathbf{1^D}]^{3+}$ is similar to that in the previously reported $[M^{II}_3(D\text{-}L^{Au_3})_2]$ (M = Co, Cu, Cd), in which each M^{II} centre is octahedrally coordinated by two *N*,*O*,*S*-chelates of D-pen from two $(D\text{-}L^{Au_3})^{3-}$ metalloligands.[36,37] However, each Ag^I centre in $[\mathbf{1^D}]^{3+}$ adopts an S_2 linear geometry coordinated by two thiolato donors, while each Cu^{II} centre has a *trans*-N_2O_3 square-pyramidal geometry coordinated by two *N*,*O*-chelates and a water molecule. In $[\mathbf{1^D}]^{3+}$, an S-bridged $Au^I_6Ag^I_3$ core is surrounded by 3 hydrophilic Cu^{II} centres with

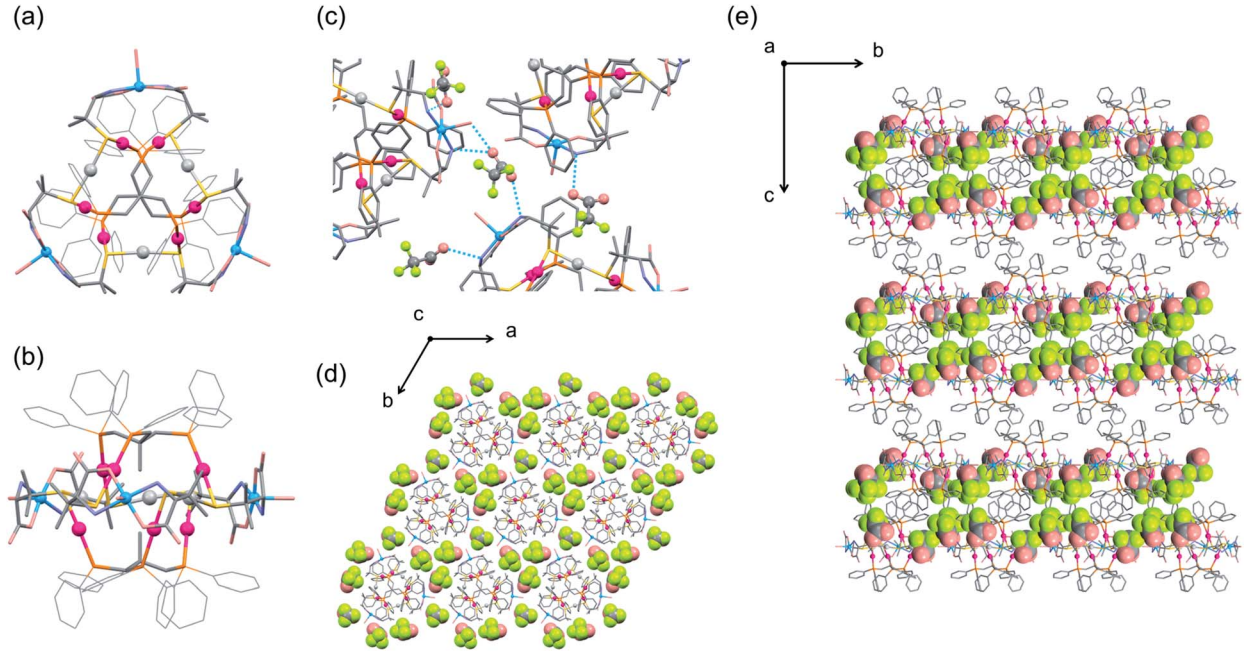

Fig. 2 Crystal structure of I′. Top (a) and side (b) views of the structure of the $[\mathbf{1}^{\mathbf{D}}]^{3+}$ complex cation. (c) Hydrogen-bonding interactions between TFA^- anions and the $[\mathbf{1}^{\mathbf{D}}]^{3+}$ complex cations. Top (d) and side (e) views of the packing structure in I′ [colour codes: red, Au; silver, Ag; blue, Cu; orange, P; yellow, S; pink, O; pale blue, N; grey, C; light yellow, F].

amine, carboxylate and aqua donors in the equatorial positions, while its apical positions are covered by 12 hydrophobic phenyl groups. Each $[\mathbf{1}^{\mathbf{D}}]^{3+}$ cation is surrounded by 9 TFA^- anions so as to construct a 2D layer structure in **I′**, which is sustained by NH···O hydrogen bonds, together with coulombic interactions (Fig. 2c and d). The 2D layers are stacked in an ABAB fashion to form CH···π interactions between tdme phenyl groups (Fig. 2e).

Formation and crystal structure of I

We observed that different blue crystals with octahedral shapes (**I**) were produced when the blue reaction solution was stored at 25 °C to accelerate evaporation after concentrating it to a small volume at 0 °C. As in the case of **I′**, **I** was characterized by IR, diffuse reflection and CD spectra (Fig. S3 and S4†), as well as X-ray fluorescence and elemental analyses, the results of which are all essentially the same as those of **I′**. Thus, **I** was also determined to have a formula of $[Ag_3Cu_3(\text{D-L}^{Au_3})_2](TFA)_3\cdot n H_2O$. However, the powder X-ray diffraction pattern of **I** differs significantly from that of **I′**, indicative of the polymorphic relationship between **I** and **I′** (Fig. S5†).

Single-crystal X-ray analysis revealed that **I** crystallized in the cubic space group $F4_132$, which is different from the trigonal space group $P321$ for **I′**. Remarkably, **I** possesses an exceptionally large crystal lattice with a cell volume of 2 171 340 Å^3, which is the largest among non-MOFs and the third largest including MOF crystals reported thus far.[27,40] While **I** afforded very weak X-ray diffraction peaks with a low resolution, comparable to those for protein crystals, we observed electron densities that match well with those of the heavy atoms (Au, Ag, Cu, S and P) in $[\mathbf{1}^{\mathbf{D}}]^{3+}$. Finally, the total structure of **I** was established by fitting the molecular structure of $[\mathbf{1}^{\mathbf{D}}]^{3+}$ obtained from the X-ray analysis of **I′**. The asymmetric unit of **I** contains one complete $[\mathbf{1}^{\mathbf{D}}]^{3+}$ cation, three half cations and a one-third unit of $[\mathbf{1}^{\mathbf{D}}]^{3+}$ cations (Fig. S6†). Thus, the total number of $[\mathbf{1}^{\mathbf{D}}]^{3+}$ cations in the unit cell was determined to be 272, based on the symmetry operation of the space group $F4_132$. In **I**, the $[\mathbf{1}^{\mathbf{D}}]^{3+}$ cations are linked through CH···π interactions between tdme phenyl groups (Fig. S7†), generating a 3D mesoporous framework with a potential porosity of 66% (Fig. 3). Based on the elemental analysis and IR spectrum, the voids of the framework are considered to be occupied by TFA^- anions and solvated water molecules. It is assumed that the concentration of the reaction solution at 25 °C results in an aqueous-rich phase due to the faster evaporation of organic solvents, leading to the hydrophobic self-assembly of $[\mathbf{1}^{\mathbf{D}}]^{3+}$ cations through CH···π interactions to crystallize the kinetic product of **I**; in contrast, the thermodynamic product of **I′** is crystallized by slower evaporation at 0 °C. It should be noted that the recrystallization of **I** from water at 0 °C afforded **I′**, while **I** was generated by recrystallizing **I′** at 25 °C.

Topological analysis[41,42] revealed that the framework in **I** adopts a 6-connected **mtn-e** net structure (Fig. 3 and S8†).[43] This topology is the same as that of the MOF in MIL-101 with the formula $[Cr_3F(H_2O)_2O(1,4\text{-bdc})_3]\cdot n H_2O$ (1,4-bdc = 1,4-benzene dicarboxylate),[26,43] replacing the trimeric building units of chromium(III) octahedra linked by 1,4-bdc anions through coordination bonds in MIL-101 by dodecanuclear $[\mathbf{1}^{\mathbf{D}}]^{3+}$ cations connected by CH···π interactions in **I**. While MIL-101 crystallized in the achiral space group $Fd\bar{3}m$ due to the achiral nature of the trimeric building units and the 1,4-bdc linkers, the homochirality of $[\mathbf{1}^{\mathbf{D}}]^{3+}$ cations with D-pen ligands led to

crystallization of **I** in the chiral space group $F4_132$. In addition, the cell volume of **I** (2 171 340 Å^3) is three times larger than that of MIL-101 (701 860 Å^3). As in MIL-101, the framework in **I** contains two types of mesoporous cages (cage **A** and cage **B**) in a 1 : 2 ratio (Fig. 3c and d). Cage **A** consists of 42 $[\mathbf{1}^{\mathbf{D}}]^{3+}$ cations with a $[3^{28}\cdot5^{12}\cdot6^4]$ face arrangement,[44] bearing 4 hexagonal windows with an internal diameter of 20.2 Å and 12 pentagonal windows with an internal diameter of 14.0 Å (Fig. 3a and b), while cage **B** consists of 30 $[\mathbf{1}^{\mathbf{D}}]^{3+}$ cations with $[3^{20}\cdot5^{12}]$ face arrangement (icosidodecahedron),[44] having 12 pentagonal windows that are shared by cages **A**. The accessible volumes of cage **A** and cage **B** in **I**, which are occupied by TFA^- anions and water molecules, are 64 000 Å^3 (internal diameter 49.7 Å) and 29 000 Å^3 (internal diameter of 38.2 Å), respectively. These are much larger than the corresponding cages in MIL-101 (20 600 Å^3 with an internal diameter of 34 Å and 12 700 Å^3 with an internal diameter of 29 Å).[26]

Anion exchange of I

In contrast to the insolubility of MIL-101 in any solvent,[26] **I** is soluble in water due to its highly porous 3D framework sustained by CH$\cdots\pi$ interactions.§ While **I** lost a crystallinity upon desolvation, its crystallinity was retained for at least several weeks without dissolving when soaked in aqueous NaTFA. This was also observed when crystals of **I** were soaked in other aqueous salts, such as NaX = $NaPF_6$, $NaBF_4$ and NaOTf (OTf = trifluoromethanesulfonate). IR spectroscopy and elemental analysis revealed that the crystals ($\mathbf{I_X}$) obtained by soaking crystals of **I** in aqueous NaX for 1 h contain only X^- as counter-anions (Fig. S9†), indicative of the complete exchange of the TFA^- anions in **I**. The retention of the single crystallinity and framework structure in **I** was confirmed by powder X-ray diffraction studies (Fig. S10†), together with single-crystal X-ray crystallography. Notably, the anion exchange of **I** was completed just by soaking the samples in

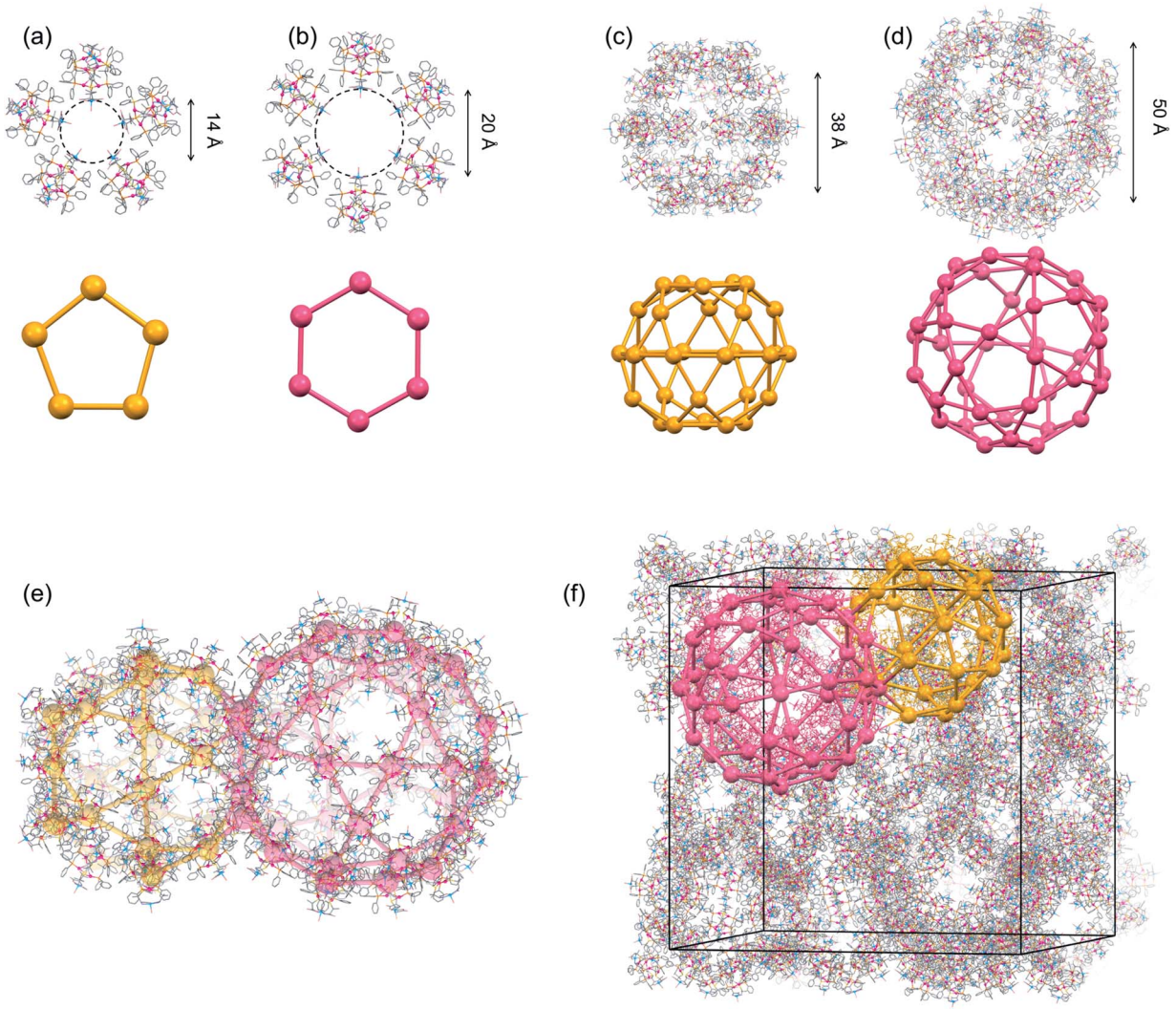

Fig. 3 Crystal structure of **I**.‡ (a) A pentagonal window in cage **A** and cage **B**. (b) A hexagonal window in cage **A**. (c) Cage **B**. (d) Cage **A**. (e) Face-sharing cage **A** and cage **B**. (f) Schematic representation of the packing structure of a 6-connected **mtn-e** net (cage **A** and cage **B** are represented by red and orange colours, respectively, with $[\mathbf{1}^{\mathbf{D}}]^{3+}$ cations shown by balls) [colour codes: red, Au; silver, Ag; blue, Cu; orange, P; yellow, S; pink, O; pale blue, N; grey, C].

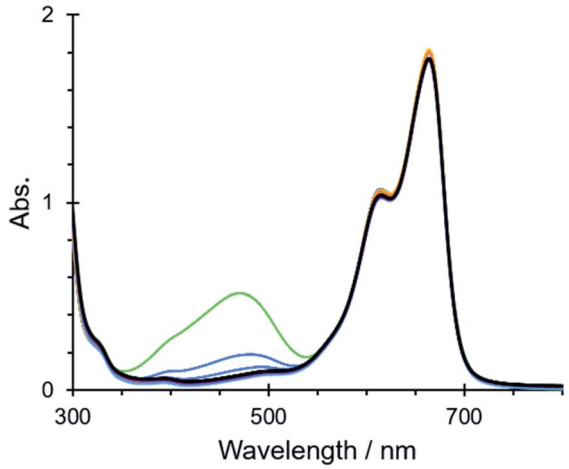

Fig. 4 Time-dependent absorption spectral change of a mixture of aqueous methyl orange (4.0×10^{-5} M, 1.5 mL) and aqueous methylene blue (a 4.0×10^{-5} M, 1.5 mL) after soaking crystals of $\mathbf{I}_{PF6}$ (*ca.* 10 mg) for 0 h (green), 1 h (blue), 2 h (yellow), 4 h (orange), 6 h (light blue), 8 h (purple) and 10 h (black).

aqueous $NaPF_6$ for 1 minute and even by washing the crystals with aqueous $NaPF_6$ on filter paper. To investigate the selective exchange of counter-anions, crystals of **I** were soaked in a 1 : 1 : 1 mixture of aqueous $NaPF_6$, $NaBF_4$ and NaOTf. Again, the single crystallinity was retained and the crystals thus obtained ($\mathbf{I}_{PF6/BF4/OTf}$) contained only PF_6^- as counter-anions. This implies that PF_6^- has a higher affinity for the cationic framework than do BF_4^- and OTf^-, presumably due to the effective formation of NH···F and Ph···F interactions with $[\mathbf{1}^{D}]^{3+}$ cations in the framework. Consistent with these results, $\mathbf{I}_{PF6}$ is much less soluble in water than **I**, $\mathbf{I}_{BF4}$ and $\mathbf{I}_{OTf}$,§ indicating that the cationic framework is reinforced by introducing PF_6^- as counter-anions.

Reinforcement of the cationic framework allowed the incorporation of the large organic anion BTB^{3-} (H_3BTB = 1,3,5-tris(4′-carboxyphenyl)benzene; Fig. S11†) with 3 carboxylate groups retaining the single crystallinity by soaking crystals of $\mathbf{I}_{PF6}$ in aqueous H_3BTB for 1 h;[45] the same treatment of crystals of **I** resulted in the loss of its crystallinity (Fig. S12†). The resulting crystals of $\mathbf{I}_{BTB}$, which are almost insoluble in water,§ are formulated as $[\mathbf{1}^{D}](BTB)_{2/3}(PF_6)$ based on the IR spectrum (Fig. S13†) and elemental analyses, suggesting the presence of PF_6^- anions that tightly interact with the cationic framework. Not only the organic BTB^{3-} but also the anionic metal-cluster $[Rh_4Zn_4O(L\text{-cys})_{12}]^{6-}$ with 12 carboxylate groups (Fig. S11†)[46,47] was quickly incorporated into the cationic framework retaining the single crystallinity *via* the partial exchange of PF_6^- anions in $\mathbf{I}_{PF6}$; soaking crystals of $\mathbf{I}_{PF6}$ in aqueous $K_6[Rh_4Zn_4O(L\text{-cys})_{12}]$ for 1 h afforded single crystals of

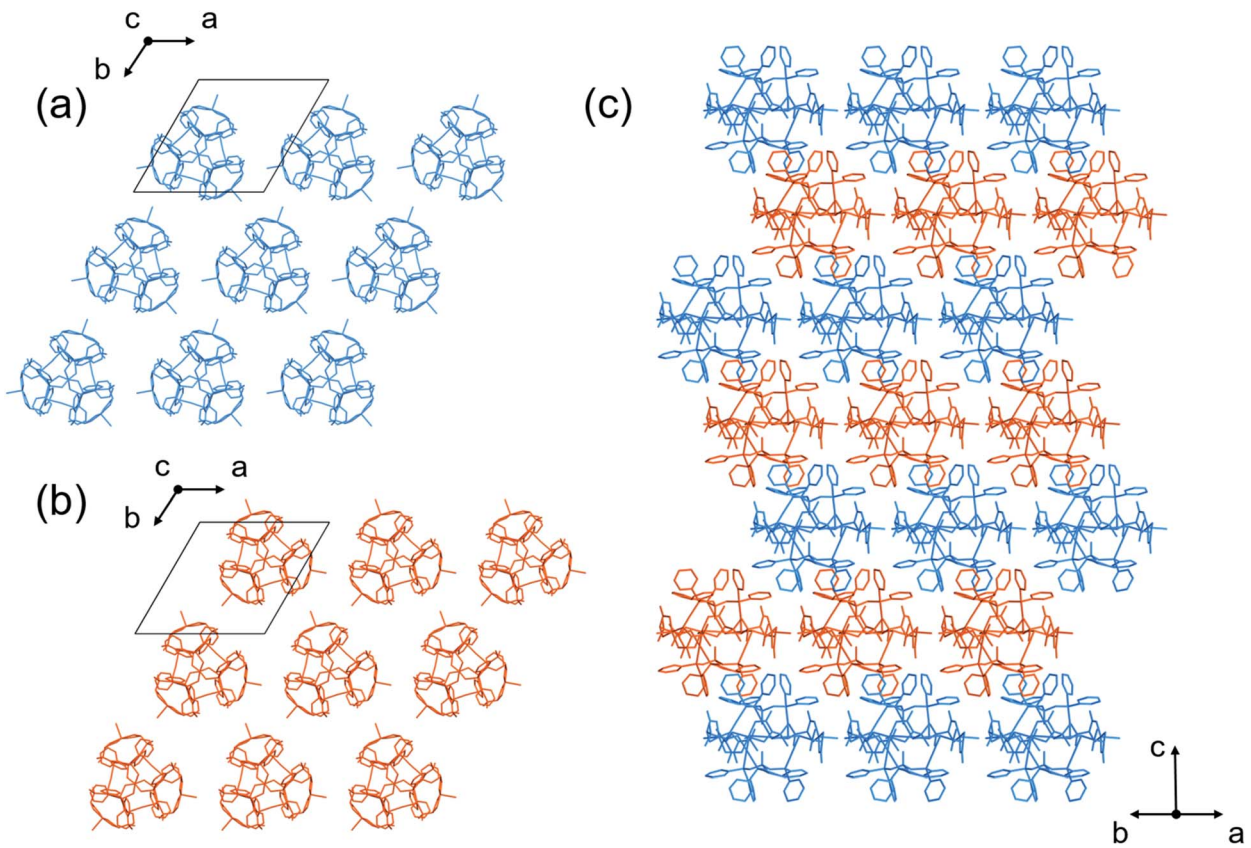

Fig. 5 Crystal structure of II′. (a) 2D layer structure composed of $[\mathbf{1}^{D}]^{3+}$ cations. (b) 2D layer structure composed of $[\mathbf{1}^{L}]^{3+}$ cations. (c) Side view of the packing structure [color codes: blue, D-$[\mathbf{1}]^{3+}$; orange, L-$[\mathbf{1}]^{3+}$].

$\mathbf{I_{RhZn}}$ formulated as $[\mathbf{1}^{\mathrm{D}}][Rh_4Zn_4O(\text{L-cys})_{12}]_{1/3}(PF_6)$, which are also insoluble in water.§¶

The cationic nature of the mesoporous framework in $\mathbf{I_{PF6}}$ also led to the quick uptake of an anionic dye of resorufin sodium salt from its aqueous solution, which was confirmed by tracing the absorption spectral change of the solution; the characteristic absorption band at 570 nm decreased with time and nearly disappeared on soaking crystals of $\mathbf{I_{PF6}}$ for 6 h (Fig. S16a†). This was also the case for another anionic dye of methyl orange,‖** but no significant uptake was observed for a neutral dye of Basic Red 5 and a cationic dye of methylene blue (Fig. S16b–d†). The uptake of an anionic dye in $\mathbf{I_{PF6}}$ is in contrast to the uptake of a cationic dye in NU-1301, which has an anionic MOF structure.[27] Note that soaking crystals of $\mathbf{I_{PF6}}$ in an aqueous solution containing methyl orange and methylene blue in a 1 : 1 ratio led to the disappearance of the absorption due to methyl orange after 6 h (Fig. 4). This result demonstrates that $\mathbf{I_{PF6}}$ has an ability to remove an anionic dye from a mixture of cationic and anionic dyes in solution.

Synthesis and crystal structures of II′ and II

As expected, the use of $[Au_3(tdme)(\text{L-Hpen})_3]$ instead of $[Au_3(\text{-tdme})(\text{D-Hpen})_3]$ led to the production of hexagonal plate crystals ($\mathbf{I'_L}$) and octahedral crystals ($\mathbf{I_L}$) of $[Ag_3Cu_3(\text{L-L}^{Au_3})_2](TFA)_3$, which correspond to **I′** and **I**, respectively. Single-crystal X-ray crystallography established that the structures of $\mathbf{I'_L}$ and $\mathbf{I_L}$ are entirely enantiomeric to those of **I′** and **I**, respectively. Next, we carried out the reactions using a 1 : 1 mixture of $[Au_3(tdme)(\text{D-}$

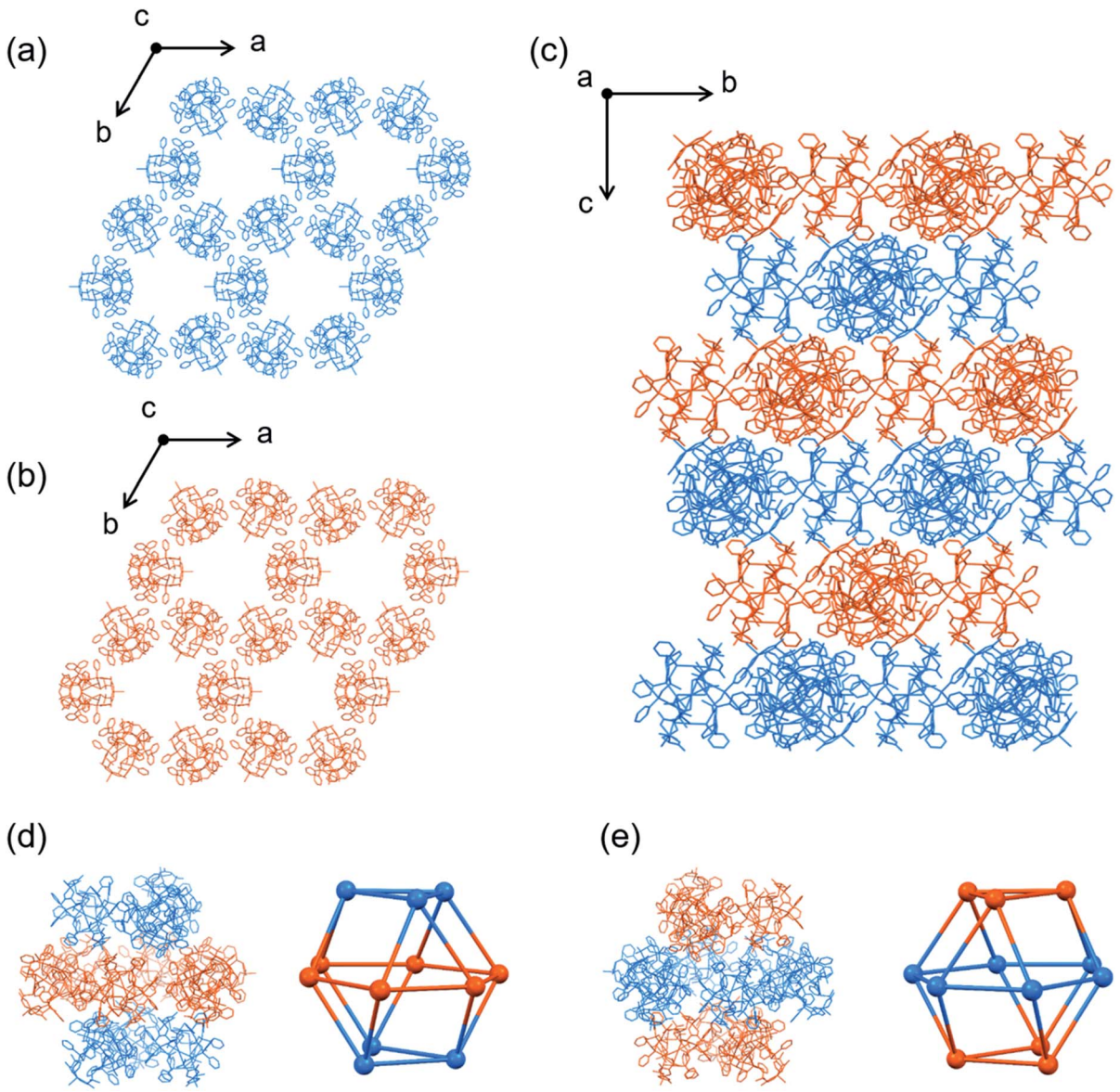

Fig. 6 Crystal structure of II. (a) 2D layer structure composed of $[\mathbf{1}^{\mathrm{D}}]^{3+}$ cations. (b) 2D layer structure composed of $[\mathbf{1}^{\mathrm{L}}]^{3+}$ cations. (c) Side view of the packing structure.†† (d and e) Enantiomeric nanoporous cages composed of $[\mathbf{1}^{\mathrm{D}}]^{3+}$ and $[\mathbf{1}^{\mathrm{L}}]^{3+}$ cations [colour codes: blue, D-$[\mathbf{1}]^{3+}$; orange, L-$[\mathbf{1}]^{3+}$].

Hpen)$_3$] (D-$H_3L^{Au_3}$) and [Au_3(tdme)(L-Hpen)$_3$] (L-$H_3L^{Au_3}$) to clarify the importance of homochirality in the creation of the highly porous structure in **I**. From this reaction, blue hexagonal plate crystals (**II′**) were produced *via* slow evaporation at 0 °C, together with blue truncated octahedral crystals (**II**) as a minor product, while fast evaporation at 25 °C dominantly yielded crystals of **II**. Based on the IR and diffuse reflection spectra (Fig. S3 and S4†), together with the X-ray fluorescence and elemental analyses, **II′** and **II** were both assigned to have the same chemical formula $[Ag^I_3Cu^{II}_3(L^{Au_3})_2](TFA)_3\cdot nH_2O$, which corresponds to those of **I′** and **I**. However, **II′** and **II** are CD silent, indicative of the presence of both D-$H_3L^{Au_3}$ and L-$H_3L^{Au_3}$ in a 1 : 1 ratio. The powder X-ray diffraction patterns of **II′** and **II** are different from each other and also different from the patterns of **I′** and **I** (Fig. S18†). Single-crystal X-ray analysis indicated that **II′** crystallized in the achiral space group of trigonal *R*3*c*. Each complex cation in **II′** consists of two homochiral metalloligands, $(D\text{-}L^{Au_3})^{3-}$ or $(L\text{-}L^{Au_3})^{3-}$, which are spanned by 3 Ag^I and 3 Cu^{II} atoms to give the homochiral $Au^I_6Ag^I_3Cu^{II}_3$ structure in $[Ag_3Cu_3(D\text{- or }L\text{-}L^{Au_3})_2(H_2O)_3]^{3+}$ ([$\mathbf{1}^{\mathbf{D}}$ or $^{\mathbf{L}}$]$^{3+}$) (Fig. S19†).

In addition, the homochiral complex cations of [$\mathbf{1}^{\mathbf{D}}$ or $^{\mathbf{L}}$]$^{3+}$ were assembled with TFA^- ions through hydrogen bonds to form a homochiral 2D layer in [$\mathbf{1}^{\mathbf{D}}$ or $^{\mathbf{L}}$](TFA)$_3$ (Fig. 5a and b). While the layer structure in **II′** is comparable to that in **I′**, the [$\mathbf{1}^{\mathbf{D}}$](TFA)$_3$ and [$\mathbf{1}^{\mathbf{L}}$](TFA)$_3$ layers are alternately, closely stacked in an off-set fashion in **II′**, resulting in an overall heterochiral structure (Fig. 5c).

II also crystallized in the achiral but different space group of trigonal $R\bar{3}c$. As those in **II′**, the homochiral $[\mathbf{1}^{\mathbf{D}}]^{3+}$ or $[\mathbf{1}^{\mathbf{L}}]^{3+}$ cations in **II** are assembled to form homochiral 2D layers (Fig. 6a and b). In **II**, however, the complex cations are linked to each other through CH$\cdots\pi$ interactions, forming hexagonal void spaces surrounded by the 6 cations in each layer (Fig. S20†). In addition, the top and bottom of the hexagonal space are each covered by 3 complex cations with opposite chirality through CH$\cdots\pi$ interactions (Fig. 6c), affording a void space surrounded by 6 $[\mathbf{1}^{\mathbf{D}}]^{3+}$ and 6 $[\mathbf{1}^{\mathbf{L}}]^{3+}$ cations in a cuboctahedral structure, which are occupied by TFA^- anions and water molecules (Fig. 6d and e). The pore volume of each cage in **II** is 16 800 Å^3 (diameter 15.9 Å) with trigonal and rhomboidal windows (diameters of 8.3 Å and 11.4 Å), which is much smaller than those of the cages in **I** (64 000 Å^3 and 29 000 Å^3). The potential porosity of **II** (35%) is also less than that of **I** (66%). Thus, the heterochiral system with a 1 : 1 mixture of $[\mathbf{1}^{\mathbf{D}}]^{3+}$ and $[\mathbf{1}^{\mathbf{L}}]^{3+}$ resulted in the creation of a less porous structure in **II** with much smaller porous cages.

Conclusions

We newly prepared the cationic $Au^I_6Ag^I_3Cu^{II}_3$ dodecanuclear complex $[Ag^I_3Cu^{II}_3(D\text{-}L^{Au_3})_2(H_2O)_3]^{3+}$ ([$\mathbf{1}^{\mathbf{D}}$]$^{3+}$) using the trigold(I) metalloligand D-$H_3L^{Au_3}$, by way of the $Au^I_6Ag^I_3$ nonanuclear complex $[Ag_3(D\text{-}H_3L^{Au_3})_2]^{3+}$. Cationic $[\mathbf{1}^{\mathbf{D}}]^{3+}$ was found to crystallize with TFA^- to produce two types of polymorph ionic crystals, **I′** and **I**, depending on the crystallization conditions; slow evaporation at 0 °C yielded the thermodynamic product of **I′** with a 2D layer structure by forming hydrogen bonds between $[\mathbf{1}^{\mathbf{D}}]^{3+}$ cations and TFA^- anions, while fast evaporation at 25 °C produced the kinetic product of **I** with a 3D porous structure consisting of CH$\cdots\pi$ interactions among $[\mathbf{1}^{\mathbf{D}}]^{3+}$ cations. The existence of hydrophobic phenyl groups at the apical positions and hydrophilic Cu^{II} moieties at their equatorial positions in $[\mathbf{1}^{\mathbf{D}}]^{3+}$ appears to be responsible for this result. Remarkably, **I** possesses a very large crystal lattice with a cell volume of more than 2 million Å^3 containing 272 $Au^I_6Ag^I_3Cu^{II}_3$ complex cations. In addition, **I** generates a mesoporous framework, the topology of which is identical to that in MIL-101, having similar but much larger two types of mesoporous cages that are occupied by counter-anions and water molecules. While MIL-101 is achiral, **I** is inherently chiral due to the presence of D-pen in $[\mathbf{1}^{\mathbf{D}}]^{3+}$. The importance of the homochiral nature of **I** in the creation of the mesoporous framework was evidenced by the employment of a racemic mixture of $[\mathbf{1}^{\mathbf{D}}]^{3+}$ and $[\mathbf{1}^{\mathbf{L}}]^{3+}$, which resulted in the construction of a less porous framework in **II**. **I** is highly soluble in water and is easily recrystallized from aqueous media. However, soaking crystals of **I** in aqueous $NaPF_6$ led to the very quick exchange of TFA^- by PF_6^- to give crystals of $\mathbf{I_{PF6}}$ retaining its single crystallinity, which is ascribed to the presence of mesoporous cages with large solvent-accessible pores. Unlike **I**, $\mathbf{I_{PF6}}$ is almost insoluble in water, indicative of the reinforcement of the porous framework *via* non-covalent interactions between $[\mathbf{1}^{\mathbf{D}}]^{3+}$ cations and PF_6^- anions. This allowed not only the incorporation of large organic and metal-cluster anions in the cationic framework to create single crystals that are entirely insoluble in water but also the selective uptake of anionic dyes from aqueous media. The controlled construction of the largest-known non-covalent mesoporous framework from a single complex salt under ambient conditions, together with its chemical modification *via* simple, very quick, single-crystal-to-single-crystal anion-exchange procedures, is expected to open up a new avenue for innovative development of porous solid materials.

Experimental

Preparation of compounds

(a) Preparation of $[Ag_3(D\text{-}H_3L^{Au_3})_2](NO_3)_3$. To a solution containing $[Au_3(tdme)(D\text{-}Hpen)_3]\cdot 5H_2O$ (D-$H_3L^{Au_3}\cdot 5H_2O$; 50 mg, 0.029 mmol) in methanol (4 mL) and acetonitrile (2 mL) was added 0.1 M AgTFA (0.45 mL, 0.045 mmol) in methanol. The mixture was stirred at 0 °C in the dark for 10 min. To the colourless solution was added 0.1 M $NaNO_3$ (1.0 mL, 0.10 mmol) in methanol. Slow evaporation of the solution at 0 °C in the dark gave colourless stick crystals, which were collected by filtration. Yield: 25 mg (43%). Anal. calcd for $[Au_6Ag_3(tdme)_2(D\text{-}Hpen)_6](NO_3)_3\cdot 17H_2O = C_{112}H_{172}Ag_3Au_6N_9O_{38}P_6S_6$: C, 32.52; H, 4.19; N, 3.05%. Found: C, 32.43; H, 4.04; N, 3.00%. IR spectrum (cm^{-1}, ATR): 1622 (ν_{COO^-}), 1098 (ν_{P-Ph}), 692 (ν_{Ph}) and 1339 (NO_3^-).

(b) Preparation of I′. To a solution containing $[Au_3(tdme)(D\text{-}Hpen)_3]\cdot 5H_2O$ (D-$H_3L^{Au_3}\cdot 5H_2O$; 50 mg, 0.029 mmol) in methanol (4 mL) and acetonitrile (2 mL) was added 0.1 M AgTFA (0.45 mL, 0.045 mmol) in methanol. The mixture was stirred at 0 °C in the dark for 10 min to give a colourless solution. To the

colourless solution were sequentially added 0.1 M *N*,*N*-diisopropylethylamine (DIPEA) (0.86 mL, 0.086 mmol) in methanol, 0.1 M aqueous $Cu(OAc)_2$ (0.45 mL, 0.045 mmol) and acetonitrile (5 mL). The mixture was stirred at 0 °C in the dark for 10 min to give a blue solution. Slow evaporation of the solution at 0 °C in the dark gave blue hexagonal plate crystals (**I′**), which were collected by filtration. Yield: 22 mg (35%). Anal. calcd for $[Au_6Ag_3Cu_3(tdme)_2(D\text{-}pen)_6(H_2O)_3](TFA)_3\cdot 8H_2O$ = $C_{118}H_{154}Ag_3Au_6Cu_3F_9N_6O_{29}P_6S_6$: C, 32.46; H, 3.56; N, 1.92%. Found: C, 32.49; H, 3.72; N, 1.96%. IR spectrum (cm^{-1}, ATR): 1633 (ν_{COO^-}), 1101 (ν_{P-Ph}), 696 (ν_{Ph}) and 1200 (ν_{TFA^-}).

Blue hexagonal plate crystals of $[Ag_3Cu_3(L\text{-}L^{Au_3})_2](TFA)_3$ (**I′$_L$**) were prepared by the same procedure as that employed for **I′**, using $[Au_3(tdme)(L\text{-}Hpen)_3]$ instead of $[Au_3(tdme)(D\text{-}Hpen)_3]$. Anal. calcd for $[Au_6Ag_3Cu_3(tdme)_2(L\text{-}pen)_6(H_2O)_3](TFA)_3\cdot 12H_2O$ = $C_{118}H_{162}Ag_3Au_6Cu_3F_9N_6O_{33}P_6S_6$: C, 31.94; H, 3.68; N, 1.89%. Found: C, 31.94; H, 3.71; N, 1.99%. IR spectrum (cm^{-1}, ATR): 1615 (ν_{COO^-}), 1102 (ν_{P-Ph}), 698 (ν_{Ph}) and 1202 (ν_{TFA^-}). Crystallographic data for **I′$_L$**: trigonal *P*321, $a = b = 19.2442(3)$ Å, $c = 26.8194(4)$ Å, $\alpha = \beta = 90°$, $\gamma = 120°$, $V = 8601.6(3)$ Å^3.

(c) Preparation of I. To a solution containing $[Au_3(tdme)(D\text{-}Hpen)_3]\cdot 5H_2O$ (50 mg, 0.029 mmol) in methanol (4 mL) and acetonitrile (2 mL) was added 0.1 M AgTFA (0.45 mL, 0.045 mmol) in methanol. The mixture was stirred at 0 °C in the dark for 10 min to give a colourless solution. To the colourless solution were sequentially added 0.1 M DIPEA (0.86 mL, 0.086 mmol) in methanol, 0.1 M aqueous solution of $Cu(OAc)_2$ (0.45 mL, 0.045 mmol) and acetonitrile (5 mL). The mixture was stirred at 0 °C in the dark for 10 min to give a blue solution. After storing the blue solution at 0 °C in the dark to be concentrated to approximately 1.5 mL, the solution was allowed to stand at 25 °C in the dark, resulting in blue octahedral crystals (**I**). After decantation, the crystals that appeared were soaked in 0.1 M aqueous NaTFA and then collected by filtration. Yield: 19 mg (29%). Anal. calcd for $[Au_6Ag_3Cu_3(tdme)_2(D\text{-}pen)_6(H_2O)_3](TFA)_3\cdot 17H_2O$ = $C_{118}H_{172}Ag_3Au_6Cu_3F_9N_6O_{38}P_6S_6$: C, 31.30; H, 3.83; N, 1.86%. Found: C, 31.28; H, 3.71; N, 1.91%. IR spectrum (cm^{-1}, ATR): 1626 (ν_{COO^-}), 1101 (ν_{P-Ph}), 692 (ν_{Ph}) and 1200 (ν_{TFA^-}).

Blue octahedral crystals of $[Ag_3Cu_3(L\text{-}L^{Au_3})_2](TFA)_3$ (**I$_L$**) were prepared by the same procedure as that employed for **I**, using $[Au_3(tdme)(L\text{-}Hpen)_3]$ instead of $[Au_3(tdme)(D\text{-}Hpen)_3]$. Anal. calcd for $[Au_6Ag_3Cu_3(tdme)_2(L\text{-}pen)_6(H_2O)_3](TFA)_3\cdot 20H_2O$ = $C_{118}H_{178}Ag_3Au_6Cu_3F_9N_6O_{41}P_6S_6$: C, 30.93; H, 3.92; N, 1.83%. Found: C, 31.17; H, 4.24; N, 1.93%. IR spectrum (cm^{-1}, ATR): 1626 (ν_{COO^-}), 1101 (ν_{P-Ph}), 692 (ν_{Ph}) and 1200 (ν_{TFA^-}). Crystallographic data for **I$_L$**: cubic $F4_132$, $a = b = c = 128.755(2)$ Å, $\alpha = \beta = \gamma = 90°$, $V = 2\,134\,481(119)$ Å^3.

(d) Preparation of I$_X$ *via* anion exchange reactions (X = PF_6^-, OTf^-, BF_4^-). Freshly prepared crystals of **I** (20 mg) were soaked in an aqueous solution containing $NaPF_6$, NaOTf or $NaBF_4$ (0.2 M, 2 mL) and then allowed to stand at 25 °C for 1 h. The resulting crystals of **I$_{PF6}$**, **I$_{OTf}$** or **I$_{BF4}$** were collected by filtration and washed with water.

Anal. **I$_{PF6}$**: calcd for $[Au_6Ag_3Cu_3(tdme)_2(D\text{-}pen)_6(H_2O)_3](PF_6)_3\cdot 18H_2O$ = $C_{112}H_{174}Ag_3Au_6Cu_3F_{18}N_6O_{33}P_9S_6$: C, 28.98; H, 3.78; N, 1.81%. Found: C, 29.01; H, 3.72; N, 1.91%. IR spectrum (cm^{-1}, ATR): 1634 (ν_{COO^-}), 1102 (ν_{P-Ph}), 697 (ν_{Ph}) and 854 ($\nu_{PF_6^-}$). Crystallographic data for **I$_{PF6}$**: cubic *F*, $a = b = c = 129.1080(20)$ Å, $\alpha = \beta = \gamma = 90°$, $V = 2\,152\,085(80)$ Å^3.

Anal. **I$_{OTf}$**: calcd for $[Au_6Ag_3Cu_3(tdme)_2(D\text{-}pen)_6(H_2O)_3](OTf)_3\cdot 18H_2O$ = $C_{115}H_{174}Ag_3Au_6Cu_3F_9N_6O_{42}P_6S_9$: C, 29.68; H, 3.77; N, 1.81%. Found: C, 29.69; H, 3.53; N, 1.87%. IR spectrum (cm^{-1}, ATR): 1634 (ν_{COO^-}), 1103 (ν_{P-Ph}), 698 (ν_{Ph}) and 1276, 1170, 1031, 640 (ν_{OTf^-}). Crystallographic data for **I$_{OTf}$**: cubic *F*, $a = b = c = 128.27(6)$ Å, $\alpha = \beta = \gamma = 90°$, $V = 2\,110\,298(1600)$ Å^3.

Anal. **I$_{BF4}$**: anal. calcd for $[Au_6Ag_3Cu_3(tdme)_2(D\text{-}pen)_6(H_2O)_3](BF_4)_3\cdot 14H_2O$ = $C_{112}H_{166}Ag_3Au_6Cu_3F_{12}N_6O_{29}P_6S_6B_3$: C, 30.61; H, 3.81; N, 1.91%. Found: C, 30.58; H, 3.67; N, 1.89%. IR spectrum (cm^{-1}, ATR): 1634 (ν_{COO^-}), 698 (ν_{Ph}) and 1102 ($\nu_{BF_4^-}$). Crystallographic data for **I$_{BF4}$**: cubic *F*, $a = b = c = 128.5(6)$ Å, $\alpha = \beta = \gamma = 90°$, $V = 2\,121\,793(19\,000)$ Å^3.

(e) Preparation of I$_{BTB}$ *via* an anion exchange reaction. Freshly prepared crystals of **I$_{PF6}$** (20 mg) were soaked in an aqueous solution containing H_3BTB (0.025 M, 2 mL), which was deprotonated by NaOH and then allowed to stand at 25 °C for 1 h. The resulting crystals of **I$_{BTB}$** were collected by filtration and washed with water. Anal. **I$_{BTB}$**: calcd for $[Au_6Ag_3Cu_3(tdme)_2(D\text{-}pen)_6(H_2O)_3](BTB)_{2/3}(PF_6)\cdot 15H_2O$ = $C_{130}H_{178}Ag_3Au_6Cu_3F_6N_6O_{34}P_7S_6$: C, 34.03; H, 3.91; N, 1.83%. Found: C, 34.05; H, 3.95; N, 1.81%. IR spectrum (cm^{-1}, ATR): 1627 (ν_{COO^-}), 698 (ν_{Ph}), 1588, 1545, 1373, 781 (ν_{BTB}) and 842 ($\nu_{PF_6^-}$). Crystallographic data for **I$_{BTB}$**: cubic $F4_132$, $a = b = c = 128.2485(23)$ Å, $\alpha = \beta = \gamma = 90°$, $V = 2\,109\,390(66)$ Å^3.

(f) Preparation of I$_{RhZn}$ *via* an anion exchange reaction. Freshly prepared crystals of **I$_{PF6}$** (20 mg) were soaked in an aqueous solution containing $K_6[Rh_4Zn_4(L\text{-}cys)_{12}O]$ (0.01 M, 1 mL) and then allowed to stand at 25 °C for 1 h. Anal. **I$_{RhZn}$**: calcd for $[Au_6Ag_3Cu_3(tdme)_2(D\text{-}pen)_6(H_2O)_3][Rh_4Zn_4(L\text{-}cys)_{12}O]_{1/3}(PF_6)\cdot 28H_2O$ = $C_{124}H_{214}Ag_3Au_6Cu_3F_6N_{10}O_{51.3}P_7Rh_{1.3}S_{10}Zn_{1.3}$: C, 28.43; H, 4.12; N, 2.67%. Found: C, 28.42; H, 4.32; N, 2.49%. IR spectrum (cm^{-1}, ATR): 1609 (ν_{COO^-}), 693 (ν_{Ph}) and 840 ($\nu_{PF_6^-}$). Crystallographic data for **I$_{RhZn}$**: cubic $F4_132$, $a = b = c = 128.3373(24)$ Å, $\alpha = \beta = \gamma = 90°$, $V = 2\,113\,774(68)$ Å^3.

(g) Preparation of II′. To a solution containing $[Au_3(tdme)(D\text{-}Hpen)_3]\cdot 5H_2O$ ($D\text{-}H_3L^{Au_3}\cdot 5H_2O$; 25 mg, 0.014 mmol) and $[Au_3(tdme)(L\text{-}Hpen)_3]\cdot 5H_2O$ ($L\text{-}H_3L^{Au_3}\cdot 5H_2O$; 25 mg, 0.014 mmol) in methanol (4 mL) and acetonitrile (2 mL) was added 0.1 M AgTFA (0.45 mL, 0.045 mmol) in methanol. The mixture was stirred at 0 °C in the dark for 10 min to give a colorless solution. To the colorless solution were sequentially added 0.1 M DIPEA (0.86 mL, 0.086 mmol) in methanol, 0.1 M aqueous solution of $Cu(OAc)_2\cdot H_2O$ (0.45 mL, 0.045 mmol) and acetonitrile (5 mL). The mixture was stirred at 0 °C in the dark for 10 min to give a blue solution. Slow evaporation of the solution at 0 °C in the dark yielded blue hexagonal plate crystals (**II′**), together with a small amount of blue truncated octahedral crystals of **II**. The resulting crystals were collected by filtration and the crystals of **II** were removed by hand. Yield: 20 mg (31%). Anal. calcd for $[Au_6Ag_3Cu_3(tdme)_2(D\text{- or }L\text{-}pen)_6(H_2O)_3](TFA)_3\cdot 15H_2O$ = $C_{118}H_{168}Ag_3Au_6Cu_3F_9N_6O_{36}P_6S_6$: C, 31.55; H, 3.77; N, 1.87%. Found: C, 31.53; H, 3.86; N, 1.94%. IR spectrum (cm^{-1}, ATR): 1624 (ν_{COO^-}), 1103 (ν_{P-Ph}), 699 (ν_{Ph}) and 1202 (ν_{TFA^-}).

(h) Preparation of II. To a colourless solution containing $[Au_3(tdme)(D\text{-}Hpen)_3]\cdot 5H_2O$ (25 mg, 0.014 mmol) and $[Au_3(tdme)(L\text{-}Hpen)_3]\cdot 5H_2O$ (25 mg, 0.014 mmol) in methanol (4 mL) and acetonitrile (2 mL) was added 0.1 M AgTFA (0.45 mL, 0.045 mmol) in methanol. The mixture was stirred at 0 °C in the dark for 10 min to give a colourless solution. To the colourless solution were sequentially added 0.1 M DIPEA (0.86 mL, 0.086 mmol) in methanol, 0.1 M aqueous solution of $Cu(OAc)_2\cdot H_2O$ (0.45 mL, 0.045 mmol) and acetonitrile (5 mL). The mixture was stirred at 0 °C in the dark for 10 min to give a blue solution. After storing the blue solution at 0 °C in the dark to be concentrated to approximately 1.5 mL, the solution was allowed to stand at 25 °C in the dark, which yielded blue truncated octahedron crystals (**II**), together with a small amount of blue hexagonal plate crystals of **II′**. The resulting crystals were collected by filtration and the crystals of **II′** were removed by hand. Yield: 12 mg (19%). Anal. calcd for $[Au_6Ag_3Cu_3(tdme)_2(D\text{- or }L\text{-}pen)_6(H_2O)_3](TFA)_3\cdot 12.5H_2O = C_{118}H_{163}Ag_3Au_6Cu_3F_9N_6O_{33.5}P_6S_6$: C, 31.87; H, 3.69; N, 1.89%. Found: C, 31.86; H, 3.68; N, 1.93%. IR spectrum (cm^{-1}, ATR): 1623 (ν_{COO^-}), 1103 ($\nu_{P\text{–}Ph}$), 698 (ν_{Ph}) and 1202 (ν_{TFA^-}).

Physical measurements

X-ray fluorescence spectrometry was performed on a SHIMADZU EDX-7000 spectrometer. IR spectra were recorded on a JASCO FT/IR-4700 infrared spectrophotometer using the ATR method at room temperature. Solid-state diffuse reflection spectra were measured on a JASCO V-670 UV/Vis/NIR spectrometer and solid-state CD spectra were recorded on a JASCO J-820 spectrometer at room temperature. Elemental analyses (C, H, N) were performed at Osaka University using a Yanaco CHN Corder MT-6. The powder X-ray diffractions were recorded at a controlled temperature in transmission mode [synchrotron radiation $\lambda = 1.0$ Å; 2θ range = 2–78°; step width = 0.01°; data collection time = 1 min] on a diffractometer equipped with a MYTHEN microstrip X-ray detector (Dectris Ltd) at the SPring-8 BL02B2 beamline. The crystals were loaded into a glass capillary tube (diameter = 0.3 mm), which was rotated during the measurements.

X-ray crystallography

The diffraction data for **I**, **II′**, $\mathbf{I_{PF6}}$, $\mathbf{I_{BTB}}$ and $\mathbf{I_{RhZn}}$ were recorded at 100 K with a PILATUS3 X CdTe 1M with synchrotron radiation ($\lambda = 0.42810$ Å) at SPring-8 (BL02B1 beamline). The diffraction images were processed by using RAPID-AUTO. The diffraction data for **II** and $[Ag_3(D\text{-}H_3L^{Au_3})_2](NO_3)_3$ were recorded at 100 K with a Rayonix MX225HS CCD area detector with synchrotron radiation ($\lambda = 0.62997$ Å for **II** and 0.6000 Å for $[Ag_3(D\text{-}H_3L^{Au_3})_2](NO_3)_3$) at the 2D beamline at the Pohang Accelerator Laboratory (PAL). The intensity data were processed using the HKL3000 program and collected by using the ω-scan technique.[48] The diffraction data for **I′**, $\mathbf{I_{Otf}}$ and $\mathbf{I_{BF4}}$ were recorded at 100 K with a hybrid pixel array detector with Mo Kα X-ray source ($\lambda = 0.71073$ Å). The diffraction images were processed by using CrysAlisPro 1.171.40.75a (Rigaku OD, 2020). The structures were solved by direct methods using SHELXS-2014.[49] The structure refinements were carried out using full-matrix least-squares (SHELXL-2018/3).[49]

For $[Ag_3(D\text{-}H_3L^{Au_3})_2](NO_3)_3$, DFIX, ISOR, DELU and SADI restraints and a FLAT constrain were applied to model nitrate anions. Global ISOR, RIGU and SIMU were applied. All nonhydrogen atoms were refined anisotropically. The contributions of undetermined NO_3^- ions and solvated water molecules were excluded using the SQUEEZE program in the PLATON package.[50] 4882 electrons were found in the void with a volume of 11 701 Å^3 per unit cell by the mask calculation. The number of electrons is not consistent with the presence of 3 NO_3^- and 34 H_2O per formula unit, which gives 3464 electrons per unit cell. The difference in the electron numbers is due to the loss of solvated water molecules in the course of the isolation of the bulk sample.

For **I**, the positions of Au, Ag, Cu, S and P atoms were solved by direct methods using SHELXS-2014 and refined by using full-matrix least-squares (SHELXL-2018/3).[49] The molecular structure of each $[\mathbf{1^D}]^{3+}$ complex-cation was fitted with that determined in **I′** by using the FRAG command and refined as a rigid body. ISOR, DELU and SIMU restraints and a EADP constrain were applied to coordinated waters. Au and Ag atoms were refined anisotropically and Cu, S, P, O, N and C atoms were refined isotropically. The exclusion of the undetermined TFA^- ions and solvated water molecules with SQUEEZE[50] was not successful.

For **I′**, DFIX, ISOR, DELU, SIMU and SADI restraints were applied to model trifluoro acetate anions. All nonhydrogen atoms except for crystal water molecules were refined anisotropically. Six diffractions were omitted to improve the data quality. 669 electrons were found in the void with a volume of 2117 Å^3 per unit cell by the mask calculation. The number of electrons is not consistent with the presence of 8 H_2O per formula unit, which gives 160 electrons per unit cell. The difference in the electron numbers is due to the loss of solvated water molecules in the course of the isolation of the bulk sample.

For **II**, ISOR, DELU and SIMU restraints were applied for coordinated water molecules. Global SIMU were applied. All nonhydrogen atoms were refined anisotropically. The contributions of undetermined TFA^- ions and solvated water molecules were excluded using the SQUEEZE program in the PLATON package.[50] Nineteen diffractions were omitted to improve the data quality. 9168 electrons were found in the void with a volume of 30 609 Å^3 per unit cell by the mask calculation. The number of electrons is not consistent with the presence of 3 TFA^- and 12.5 H_2O per formula unit, which gives 5220 electrons per unit cell. The difference in the electron numbers is due to the loss of solvated water molecules in the course of the isolation of the bulk sample.

For **II′**, DFIX, ISOR, DELU, SIMU, RIGU and SADI restraints were applied to model trifluoro acetate anions and parts of $[\mathbf{1^D}]^{3+}$ complex-cation. All nonhydrogen atoms were refined anisotropically. Two diffractions were omitted to improve the data quality. The exclusion of the undetermined TFA^- ions and solvated water molecules with SQUEEZE was not successful. 1685 electrons were found in the void with a volume of 6288 Å^3

per unit cell by the mask calculation. The number of electrons is compatible with the presence of 2 TFA^- and 15 H_2O per formula unit, which gives 1560 electrons per unit cell.

Topological analysis

The **mtn-e** topology was identified using ToposPro (Ver. 5.3.3.3).[41,42] An $Au^I_6Ag^I_3Cu^{II}_3$ dodecanuclear complex and CH$\cdots\pi$ contacts between two complexes were simplified as a node and a single edge, respectively.

Author contributions

H. T. performed the syntheses and spectroscopic measurements on the compounds; T. Kojima performed single X-ray diffraction analyses. T. Kojima, N. Y. and T. Konno wrote the manuscript; T. Konno conceived and designed the project. All authors discussed the results and commented on the manuscript.

Conflicts of interest

There are no conflicts to declare.

Acknowledgements

This work was supported by JST CREST (Grant No. JPMJCR13L3) and JSPS KAKENHI (Grant No. 18H05344, 19K05496 and 20K05664). The synchrotron radiation experiments were performed at the BL02B1 and BL02B2 beamlines of SPring-8 with the approval of JASRI (Proposal No. 2018B1481, 2019A1302 and 2019A1350) and at the 2D-SMC beamline of the Pohang Accelerator Laboratory. We would like to thank Mr Kyohei Adachi for a part of the anion-exchange experiments.

Notes and references

‡ The TFA^- anions and solvated water molecules that might be highly disordered in **I** were not located due to the weak electron densities and the very large cell volume of **I**.

§ The solubilities of crystals in water at room temperature were evaluated to be 0.7 mg mL^{-1}, 0.4 mg mL^{-1}, and 0.3 mg mL^{-1} for $\mathbf{I_{PF6}}$, $\mathbf{I_{RhZn}}$, and $\mathbf{I_{BTB}}$, respectively, based on the absorption spectral measurements.

¶ The presence of the $Rh^{III}_4Zn^{II}_4$ cluster anions in $\mathbf{I_{RhZn}}$, together with PF_6^-, was confirmed by the IR spectrum (Fig. S14†) and the X-ray fluorescence and elemental analyses, together with the solid-state CD spectra (Fig. S15†).

‖ The PXRDs of $\mathbf{I_{PF6}}$ were much broaden after the uptake of methyl orange, which is indicative of the partial collapse of the cationic framework (Fig. S12d†).

** The adsorbed methyl orange was removal from the crystals by soaking in 0.2 M aqueous $NaPF_6$, which was confirmed by the absorption spectral measurements (Fig. S17†).

†† The TFA^- anions and solvated water molecules were not located due to their positional disorder.

1 J. Y. Lee, O. K. Farha, J. Roberts, K. A. Scheidt, S. B. T. Nguyen and J. T. Hupp, *Chem. Soc. Rev.*, 2009, **38**, 1450.
2 Q. Wang and D. Astruc, *Chem. Rev.*, 2020, **120**, 1438.
3 J. L. C. Rowsell and O. M. Yaghi, *Microporous Mesoporous Mater.*, 2004, **73**, 3.
4 S. Horike, S. Shimomura and S. Kitagawa, *Nat. Chem.*, 2009, **1**, 695.
5 T. A. Makal, J.-R. Li, W. Lu and H.-C. Zhou, *Chem. Soc. Rev.*, 2012, **41**, 7761.
6 H. Li, K. Wang, Y. Sun, C. T. Lollar, J. Li and H.-C. Zhou, *Mater. Today*, 2018, **21**, 108.
7 L. Gao, C.-Y. V. Li, K.-Y. Chan and Z.-N. Chen, *J. Am. Chem. Soc.*, 2014, **136**, 7209.
8 G. Distefano, H. Suzuki, M. Tsujimoto, S. Isoda, S. Bracco, A. Comotti, P. Sozzani, T. Uemura and S. Kitagawa, *Nat. Chem.*, 2013, **5**, 335.
9 J. D. Evans, V. Bon, I. Senkovska, H.-C. Lee and S. Kaskel, *Nat. Commun.*, 2020, **11**, 2690.
10 L. Liu, Y. Song, H. Chong, S. Yang, J. Xiang, S. Jin, X. Kang, J. Zhang, H. Yua and M. Zhu, *Nanoscale*, 2016, **8**, 1407.
11 Y. Inokuma, T. Arai and M. Fujita, *Nat. Chem.*, 2010, **2**, 780.
12 Y. Inokuma, S. Yoshioka, J. Ariyoshi, T. Arai, Y. Hitora, K. Takada, S. Matsunaga, K. Rissanen and M. Fujita, *Nature*, 2013, **495**, 461.
13 M. Hoshino, A. Khutia, H. Xing, Y. Inokuma and M. Fujita, *IUCrJ*, 2016, **3**, 139.
14 H.-L. Lu, D.-Q. Lin, M.-M. Zhu and S.-J. Yao, *J. Sep. Sci.*, 2012, **35**, 2131.
15 K. Ariga, A. Vinu, Y. Yamauchi, Q. Ji and J. P. Hill, *Bull. Chem. Soc. Jpn.*, 2011, **85**, 1.
16 Z. Wu and D. Zhao, *Chem. Commun.*, 2011, **47**, 3332.
17 A. Walcarius, *Chem. Soc. Rev.*, 2013, **42**, 4098.
18 W. Li, J. Liu and D. Zhao, *Nat. Rev. Mater.*, 2016, **1**, 16023.
19 M. Eddaoudi, J. Kim, N. Rosi, D. Vodak, J. Wachter, M. O'Keeffe and O. M. Yaghi, *Science*, 2002, **295**, 469.
20 L. Song, J. Zhang, L. Sun, F. Xu, F. Li, H. Zhang, X. Si, C. Jiao, Z. Li, S. Liu, Y. Liu, H. Zhou, D. Sun, Y. Du, Z. Cao and Z. Gabelica, *Energy Environ. Sci.*, 2012, **5**, 7508.
21 W. Xuan, C. Zhu, Y. Liu and Y. Cui, *Chem. Soc. Rev.*, 2012, **41**, 1677.
22 H. Deng, S. Grunder, K. E. Cordova, C. Valente, H. Furukawa, M. Hmadeh, F. Gándara, A. C. Whalley, Z. Liu, S. Asahina, H. Kazumori, M. O'Keeffe, O. Terasaki, J. F. Stoddart and O. M. Yaghi, *Science*, 2012, **336**, 1018.
23 X. Lian, Y. Fang, E. Joseph, Q. Wang, J. Li, S. Banerjee, C. Lollar, X. Wang and H.-C. Zhou, *Chem. Soc. Rev.*, 2017, **46**, 3386.
24 D. Liu, D. Zou, H. Zhu and J. Zhang, *Small*, 2018, **14**, 1801454.
25 H. Y. Guan, R. J. LeBlanc, S. Y. Xie and Y. F. Yue, *Coord. Chem. Rev.*, 2018, **369**, 76.
26 G. Férey, C. Mellot-Draznieks, C. Serre, F. Millange, J. Dutour, S. Surblé and I. Margiolaki, *Science*, 2005, **309**, 2040.
27 P. Li, N. A. Vermeulen, C. D. Malliakas, D. A. Gómez-Gualdrón, A. J. Howarth, B. L. Mehdi, A. Dohnalkova, N. D. Browning, M. O'Keeffe and O. K. Farha, *Science*, 2017, **356**, 624.
28 A. P. Côté, H. M. El-Kaderi, H. Furukawa, J. R. Hunt and O. M. Yaghi, *J. Am. Chem. Soc.*, 2007, **129**, 12914.
29 S. Y. Ding and W. Wang, *Chem. Soc. Rev.*, 2013, **42**, 548.
30 Q. Yin, P. Zhao, R.-J. Sa, G.-C. Chen, J. Lü, T.-F. Liu and R. Cao, *Angew. Chem., Int. Ed.*, 2018, **57**, 7691.
31 M. J. Białek and R. Klajn, *Chem*, 2019, **5**, 2283.

32 R. Lin, Y. He, P. Li, H. Wang, W. Zhou and B. Chen, *Chem. Soc. Rev.*, 2019, **48**, 1362.
33 Q. Huang, W. Li, Z. Mao, L. Qu, Y. Li, H. Zhang, T. Yu, Z. Yang, J. Zhao, Y. Zhang, M. P. Aldred and Z. Chi, *Nat. Commun.*, 2019, **10**, 3074.
34 K. Ma, P. Li, J. H. Xin, Y. Chen, Z. Chen, S. Goswami, X. Liu, S. Kato, H. Chen, X. Zhang, J. Bai, M. C. Wasson, R. R. Maldonado, R. Q. Snurr and O. K. Farha, *Cell Rep. Phys. Sci.*, 2020, **1**, 100024.
35 B. Wang, X.-L. Lv, J. Lv, L. Ma, R.-B. Lin, H. Cui, J. Zhang, Z. Zhang, S. Xiang and B. Chen, *Chem. Commun.*, 2020, **56**, 66.
36 Y. Hashimoto, N. Yoshinari, N. Matsushita and T. Konno, *Eur. J. Inorg. Chem.*, 2014, 3474.
37 K. Imanishi, B. Wahyudianto, T. Kojima, N. Yoshinari and T. Konno, *Chem.–Eur. J.*, 2020, **26**, 1827.
38 N. Yoshinari and T. Konno, *Chem. Rec.*, 2016, **16**, 1647.
39 J. Ribas Gispert, *Coordination Chemistry*, Wiley-VCH, Weinheim, 2008.
40 X. Lian, Y.-P. Chen, T.-F. Liu and H.-C. Zhou, *Chem. Sci.*, 2016, **7**, 6969.
41 V. A. Blatov, *Crystallogr. Rev.*, 2004, **10**, 249.
42 V. A. Blatov, *IUCr CompComm Newsletter*, 2006, **7**, 4.
43 D. Kim, X. Liu and M. S. Lah, *Inorg. Chem. Front.*, 2015, **2**, 336.
44 V. A. Blatov, D. M. Proserpio and M. O'Keeffe, *CrystEngComm*, 2010, **12**, 44.
45 E. Weber, M. Hecker, E. Koepp, W. Orlia, M. Czugler and I. Csöregh, *J. Chem. Soc., Perkin Trans. 2*, 1988, 1251.
46 T. Konno, K. Okamoto and J. Hidaka, *Inorg. Chem.*, 1994, **33**, 538.
47 N. Yoshinari, S. Yamashita, Y. Fukuda, Y. Nakazawa and T. Konno, *Chem. Sci.*, 2019, **10**, 587.
48 W. Minor, M. Cymborowski, Z. Otwinowski and M. Chruszcz, *Acta Crystallogr., Sect. D: Biol. Crystallogr.*, 2006, **62**, 859.
49 G. Sheldrick, *Acta Crystallogr., Sect. A: Found. Crystallogr.*, 2008, **64**, 112.
50 A. L. Spek, *Acta Crystallogr., Sect. B: Struct. Sci.*, 2009, **65**, 148.